Discontinuous Galerkin Method for Atmospheric Modeling

Ram Nair

(rnair@ucar.edu)

Scientific Computing Division (NCAR)

April 26, 2005

Discontinuous Galerkin Method (DGM)

- Motivation
- DGM in Cartesian Geometry
  - DGM in 1D (Algorithm)
  - Modal & Nodal versions
- Extension of DGM to 2D
  - Cartesian Geometry
  - Spherical Geometry (Cubed-Sphere)
- Flux form SW Model
- Numerical experiments & Results
- Parallel Implementation
- Summary

DGM: Motivation

- DGM may be considered as a hybrid approach combining the finite-volume and finite-element methods.

DGM: Motivation

- DGM may be considered as a hybrid approach combining the finite-volume and finite-element methods.
- Advantage:

DGM: Motivation

- DGM may be considered as a hybrid approach combining the finite-volume and finite-element methods.
- Advantage:
  - Inherently conservative (Monotonic option)

DGM: Motivation

- DGM may be considered as a hybrid approach combining the finite-volume and finite-element methods.
- Advantage:
  - Inherently conservative (Monotonic option)
  - High-order accuracy & High parallel efficiency

DGM: Motivation

- DGM may be considered as a hybrid approach combining the finite-volume and finite-element methods.
- Advantage:
  - Inherently conservative (Monotonic option)
  - High-order accuracy & High parallel efficiency
  - “Local” method & AMR capable

DGM: Motivation

- DGM may be considered as a hybrid approach combining the finite-volume and finite-element methods.
- Advantage:
  - Inherently conservative (Monotonic option)
  - High-order accuracy & High parallel efficiency
  - “Local” method & AMR capable
- Potential: Application in climate and atmospheric chemistry modeling, and NH modeling.

DGM: Motivation

- DGM may be considered as a hybrid approach combining the finite-volume and finite-element methods.
- Advantage:
  - Inherently conservative (Monotonic option)
  - High-order accuracy & High parallel efficiency
  - “Local” method & AMR capable
- Potential: Application in climate and atmospheric chemistry modeling, and NH modeling.
- Popular in CFD and other engineering applications *(Cockburn and Shu 1989-98)*.

DGM: Motivation

- DGM may be considered as a hybrid approach combining the finite-volume and finite-element methods.
- Advantage:
  - Inherently conservative (Monotonic option)
  - High-order accuracy & High parallel efficiency
  - “Local” method & AMR capable
- Potential: Application in climate and atmospheric chemistry modeling, and NH modeling.
- Popular in CFD and other engineering applications *(Cockburn and Shu 1989-98)*.
- Global SW model: *Giraldo et al. (JCP, 2002)*; *Nair, Thomas & Loft (MWR, 2005)*.

DGM in 1D

- 1D scalar conservation law:

$$\frac{\partial U}{\partial t} + \frac{\partial F(U)}{\partial x} = 0 \quad \text{in} \quad \Omega \times (0, T),$$

$$\text{with initial condition} \quad U_0(x) = U(x, t = 0), \quad \forall x \in \Omega$$

- The domain Ω (periodic) is partitioned into N_x non-overlapping elements (intervals) $I_j = [x_{j-1/2}, x_{j+1/2}]$, $j = 1, \ldots, N_x$, and $\Delta x_j = (x_{j+1/2} - x_{j-1/2})$

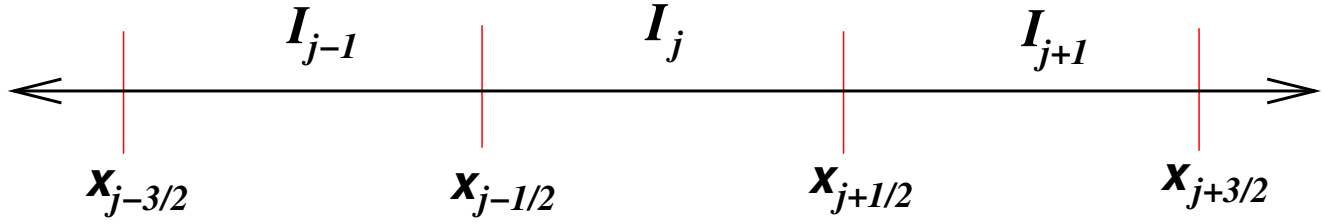

DGM-1D: Weak Formulation

- A weak formulation of the problem is obtained by multiplying the PDE by a *test* function $\varphi(x)$ and integrating over an element I_j:

$$\int_{I_j} \left[\frac{\partial U}{\partial t} + \frac{\partial F(U)}{\partial x} \right] \varphi(x) dx = 0.$$

Integrating the second term by parts $\Longrightarrow$

$$\int_{I_j} \frac{\partial U(x,t)}{\partial t} \varphi(x) dx - \int_{I_j} F(U(x,t)) \frac{\partial \varphi(x)}{\partial x} dx +$$
$$F(U(x_{j+1/2},t)) \varphi(x^-_{j+1/2}) - F(U(x_{j-1/2},t)) \varphi(x^+_{j-1/2}) = 0,$$

where $\varphi(x^-)$ and $\varphi(x^+)$ denote "left" and "right" limits

DGM-1D: Flux term

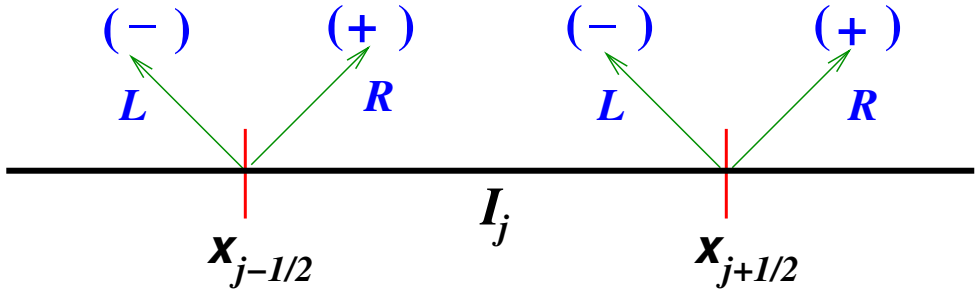

- Flux function $F(U)$ is not uniquely defined at $x_{j\pm1/2}$
- $F(U)$ is replaced by a numerical flux function $\hat{F}(U)$, dependent on the left and right limits of the discontinuous function U. At the interface $x_{j+1/2}$,

$$\hat{F}(U)_{j+1/2}(t) = \hat{F}(U(x^-_{j+1/2}, t), U(x^+_{j+1/2}, t))$$

- Typical flux formulae: Gudunov, Lax-Friedrichs, Roe, HLLC, etc.

DGM-1D: LF Flux

- For the present study, Lax-Friedrichs numerical flux is used:

$$\hat{F}(a,b) = \frac{1}{2}\left[F(a) + F(b) - \overline{\alpha}(b-a)\right],$$

where $\overline{\alpha}$ is the upper bound on $|F'(U)|$.

- Space discretization:

Let V_h^k be a finite dimensional space such that $V_h^k = \{p : p|_{I_j} \in \mathbb{P}_k(I_j)\}$ where $\mathbb{P}_k(I_j)$ is the space of polynomials in I_j of degree at most k, $\forall\, j = 1, \ldots, N_x$.

- The approximate solution $U_h(x,t) \approx U(x,t)$ and the test function $\varphi_h = \varphi$ are in V_h^k.

DGM-1D: Space Discretization

$$\int_{I_j} \frac{\partial U_h(x,t)}{\partial t}\,\varphi_h(x)dx = \int_{I_j} F(U_h(x,t))\,\frac{\partial \varphi_h(x)}{\partial x}\,dx -$$

$$\left[\hat{F}(U_h)_{j+1/2}(t)\,\varphi_h(x^-_{j+1/2}) + \hat{F}(U_h)_{j-1/2}(t)\,\varphi_h(x^+_{j-1/2})\right],$$

- Choose an orthogonal basis set spanning the space V_h^k. A set of Legendre polynomials, $\mathcal{B} = \{P_\ell(\xi), \ell = 0, 1, \ldots, k\}$ is a good compramise between accuracy and efficiency.
- Use a high-order Gaussian quadrature rule to evaluate the integrals, and that defines the computational grid.
- For the present study, the Gauss-Lobatto-Legendre (GLL) quadrature rule is employed.

DGM-1D: Space Discretization

- Map every element I_j onto the reference element $[-1,+1]$.
- Introduce a local coordinate $\xi \in [-1,+1]$ s.t.,

$$\xi = \frac{2\,(x - x_j)}{\Delta x_j},\; x_j = (x_{j-1/2} + x_{j+1/2})/2 \;\Rightarrow\; \frac{\partial}{\partial x} = \frac{2}{\Delta x_j}\,\frac{\partial}{\partial \xi}.$$

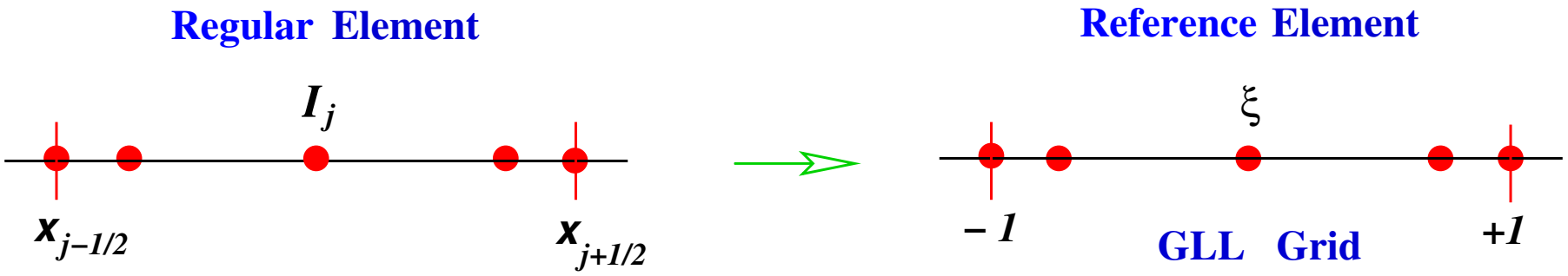

DGM-1D: Discretization (Modal)

- For every element I_j, the approximate solution $U_j(\xi, t)$, can be expressed in terms of the variable ξ:

$$U_j(\xi, t) = \sum_{\ell=0}^{k} U_j^{\ell}(t)\, P_{\ell}(\xi) \quad \text{for} \quad \xi \in [-1, 1], \quad \text{where}$$

$$U_j^{\ell}(t) = \frac{2\ell + 1}{2} \int_{-1}^{1} U_j(\xi, t)\, P_{\ell}(\xi)\, d\xi \quad \ell = 0, 1, \ldots, k.$$

- By using the properties of the Legendre polynomials

$$\int_{-1}^{1} P_{\ell}(\xi)\, P_m(\xi)\, d\xi = \frac{2}{2\ell + 1}\, \delta_{\ell m}, \quad \text{and}$$

$$P_{\ell}(1) = 1,\ P_{\ell}(-1) = (-1)^{\ell}$$

DGM-1D: ODE (Modal)

- Semi-discretized form $\Longrightarrow$

$$\frac{d}{dt}U_j^\ell(t) = \frac{2\,\ell+1}{\Delta x_j}\left[\int_{-1}^{1} F(U_j(\xi,t))\,\frac{\partial P_\ell(\xi)}{\partial \xi}\;d\xi - \left(\hat{F}(U_j(1))(t) - (-1)^\ell \hat{F}(U_j(-1))(t)\right)\right]$$

- Map from spectral to physical space ($U_j^\ell(t) \Rightarrow U_j(t)$)
- The final approximation can be expressed as

$$\frac{d}{dt}U_j = \mathcal{L}(U_j) \quad \text{in} \quad (0,T)$$

DGM-1D: Modal Vs Nodal

- The nodal basis set is constructed using Lagrange-Legendre polynomials ($h_i(\xi)$) with roots at Gauss-Lobatto quadrature points.

$$U_j(\xi) = \sum_{j=0}^{k} U_j \, h_j(\xi) \quad \text{for} \quad -1 \leq \xi \leq 1,$$

$$h_j(\xi) = \frac{(\xi^2 - 1) \, P_k'(\xi)}{k(k+1) \, P_k(\xi_j) \, (\xi - \xi_j)}.$$

- Semi-discretized form $\Longrightarrow$

$$\frac{d}{dt} U_j = \mathcal{L}(U_j) \quad \text{in} \quad (0, T)$$

Modal vs Nodal

1D basis function for an expansion of order $N = 4$

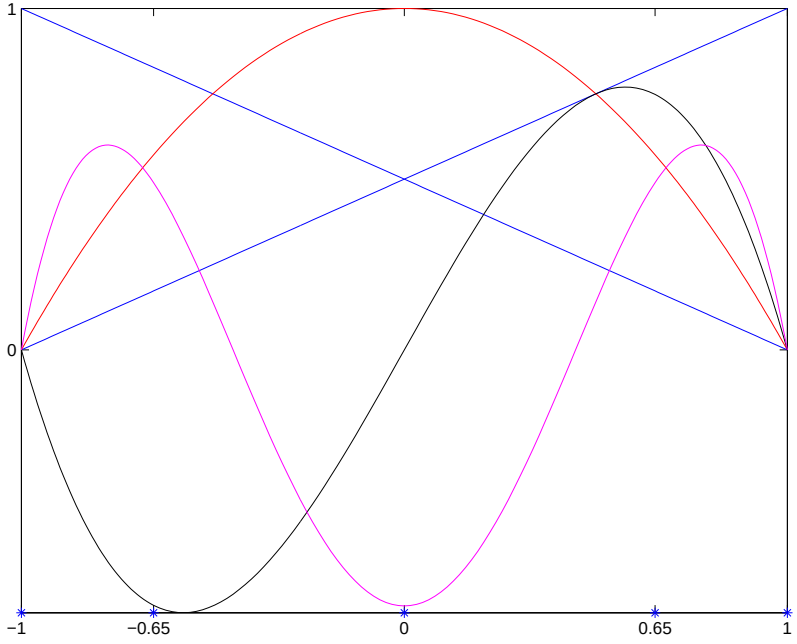

Modal Basis

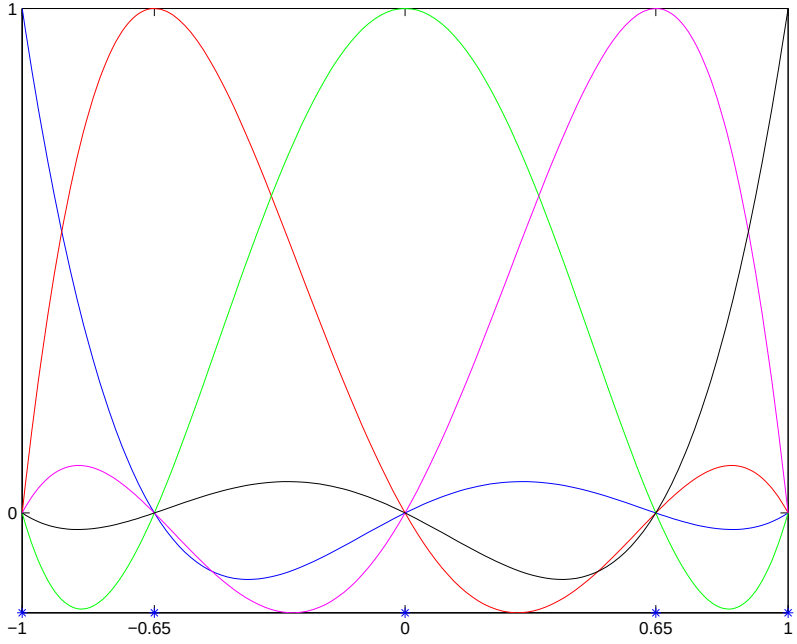

Nodal Basis

Time Integration

- Total variation diminishing third-order Runge-Kutta (TVD-RK) scheme (*Gottlieb et al., 2001*)

$$
\begin{aligned}
U^{(1)} &= U^n + \Delta t \mathcal{L}(U^n) \\
U^{(2)} &= \frac{3}{4}U^n + \frac{1}{4}U^{(1)} + \frac{1}{4}\Delta t \mathcal{L}(U^{(1)}) \\
U^{n+1} &= \frac{1}{3}U^n + \frac{2}{3}U^{(2)} + \frac{2}{3}\Delta t \mathcal{L}(U^{(2)}).
\end{aligned}
$$

  where the superscripts n and $n+1$ denote time levels t and $t + \Delta t$, respectively

- Note: The Courant number for the DG scheme is estimated to be $1/(2k+1)$, where k is the degree of the polynomial, however, no theoretical proof exists when $k > 1$ (*Cockburn and Shu, 1989*).

DG-1D: Numerical Examples

$U_t + F_x(U) = 0$, $\Omega \equiv [-1, 1]$, periodic domain. For linear advection (Gaussian-hill) $F(U) = U$, and for the Burgers Eqn. $F(U) = U^2/2$.

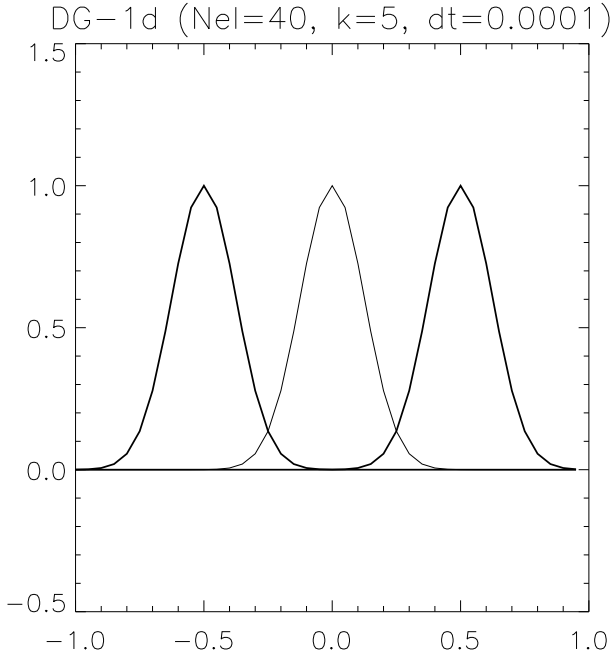

Numerical & Exact Solution

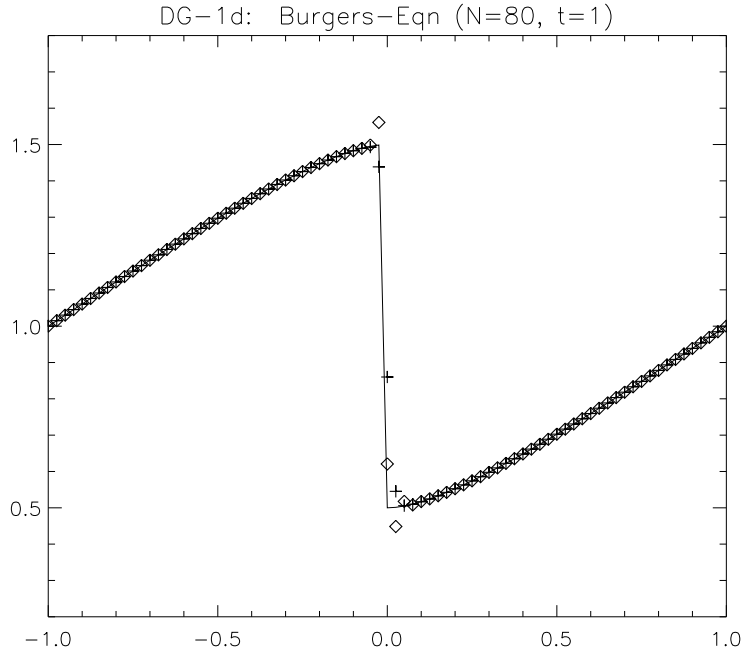

Numerical solution

DGM in 2D

- 2D scalar conservation law

$$\frac{\partial U}{\partial t} + \nabla \cdot \vec{\mathcal{F}}(U) = S(U), \quad \text{in} \quad \Omega \times (0,T); \forall\,(x,y) \in \Omega$$

where $U = U(x,y,t)$, $\nabla \equiv (\partial/\partial x, \partial/\partial y)$, $\vec{\mathcal{F}} = (F,G)$ is the flux function, and S is the source term.

- Domain: The domain Ω is partitioned into $N_x \times N_y$ rectangular non-overlapping elements Ω_{ij} such that

$$\Omega_{ij} = \{(x,y)\,|\,x \in [x_{i-1/2}, x_{i+1/2}],\ y \in [y_{j-1/2}, y_{j+1/2}]\},$$
$$\text{for} \quad i = 1,2,\ldots,N_x; \quad j = 1,2,\ldots,N_y.$$

Weak Galerkin Formulation

- Consider an element Ω_{ij} and an approximate solution U_h in the finite dimensional vector space $\mathcal{V}_h(\Omega)$.
- Multiplication of the basic equation by a test function $\varphi_h \in \mathcal{V}_h$ and integration over the element Ω_{ij} by parts, results in a weak Galerkin formulation of the problem:

$$\frac{\partial}{\partial t}\int_{\Omega_{ij}} U_h\,\varphi_h\,d\Omega - \int_{\Omega_{ij}} \vec{\mathcal{F}}(U_h)\cdot\nabla\varphi_h\,d\Omega + \int_{\partial\Omega_{ij}} \vec{\mathcal{F}}(U_h)\cdot\vec{n}\,\varphi_h\,ds = \int_{\Omega_{ij}} S(U_h)\,\varphi_h d\Omega$$

where $\vec{\mathcal{F}}(U_h)\cdot\vec{n}$ is analytic flux and $\vec{n}$ is the outward-facing unit normal vector on the element boundary $\partial\Omega_{ij}$.

DGM: Flux term

- Along the boundaries of an element $\partial\Omega_{ij}$, the function U_h is discontinuous.
- Therefore, the analytic flux $\mathcal{F}(U_h) \cdot \vec{n}$ must be replaced by a numerical flux $\widehat{\mathcal{F}}\left(U_h^-, U_h^+\right)$
- U_h^- and U_h^+ are the left and right limits of the discontinuous function U_h

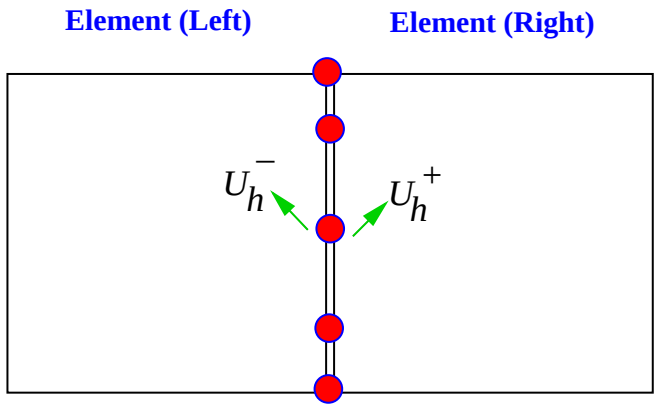

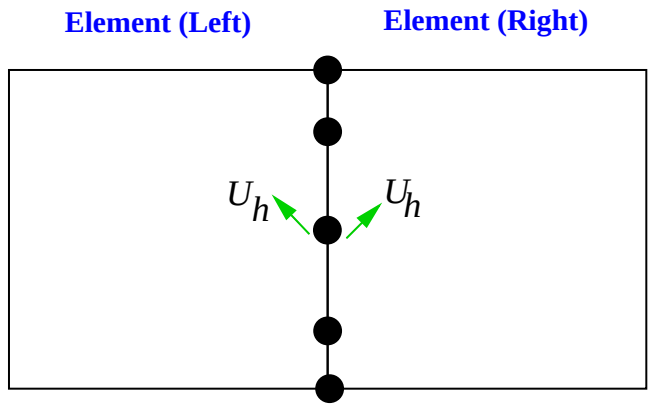

After Num. Flux Operation

DGM: Numerical Flux

- Numerical flux resolves the discontinuity of the element edges and provides only mechanism by which adjacent element interact.
- A variety of numerical flux schemes are available for the Reimann problem (*Cockburn & Shu, 2001*).
- For simplicity, the Lax-Friedrichs numerical flux is used:

$$\widehat{\mathcal{F}}(U_h^-, U_h^+) = \frac{1}{2}\left[(\mathcal{F}(U_h^-) + \mathcal{F}(U_h^+)) \cdot \vec{n} - \alpha(U_h^+ - U_h^-)\right],$$

- For a system, α is the upper bound for the absolute value of eigenvalues of the flux Jacobian $\mathcal{F}'(U)$.

Discretization (Modal)

- Choose a modal (orthogonal) basis as a set of Legendre polynomials, $\mathcal{B} = \{P_\ell(\xi), \ell = 0, 1, \ldots, N\}$
- Map $(x, y) \Rightarrow (\xi, \eta) \in [-1, 1] \otimes [-1, 1]$, reference element such that $\xi = 2(x - x_i)/\Delta x_i, \quad \eta = 2(y - y_j)/\Delta y_j$.
- Expand approximate solution U_{ij} and test function in terms of tensor-product functions from the basis set.

$$U_{ij}(\xi, \eta, t) = \sum_{\ell=0}^{N} \sum_{m=0}^{N} \hat{U}_{ij\ell m}(t)\, P_\ell(\xi)\, P_m(\eta), \qquad \text{where}$$

$$\hat{U}_{ij\ell m}(t) = \frac{(2\,\ell + 1)(2\,m + 1)}{4} \int_{-1}^{1} \int_{-1}^{1} U(\xi, \eta, t)\, P_\ell(\xi)\, P_m(\eta)\, d\xi\, d\eta.$$

Discretization (Nodal)

- The nodal basis set is constructed using a tensor-product of Lagrange-Legendre polynomials ($h_i(\xi)$) with roots at Gauss-Lobatto quadrature points.

$$U_{ij}(\xi,\eta) = \sum_{i=0}^{N}\sum_{j=0}^{N} U_{ij}\, h_i(\xi)\, h_j(\eta) \quad \text{for} \quad -1 \le \xi,\eta \le 1,$$

$$h_i(\xi) = \frac{(\xi^2-1)\, P_N'(\xi)}{N(N+1)\, P_N(\xi_i)\, (\xi-\xi_i)}.$$

- Final form for the modal discretization

$$\frac{d}{dt}\hat{U}_{ij\ell m}(t) = \frac{(2\,\ell+1)(2\,m+1)}{2\,\Delta x_i\,\Delta y_j}\left[I_{Grad} + I_{Flux} + I_{Source}\right],$$

Time integration

- Evaluate the integrals (RHS) using GLL quadrature rule.
- Solve the ODE

$$\frac{d}{dt}U = L(U) \quad \text{in} \quad (0,T)$$

- A third-order total variation diminishing (TVD) Runge-Kutta scheme (same as in the case of 1D) without a filter or limiter.

2D Cartesian: Solid-body rotation test

Gaussian-Hill: $U(x,y) = a_0 \exp(-r^2)$, $r^2 = (x-\pi/2)^2 + y^2$,
$\Omega \equiv [-\pi, \pi]^2$ (400 elements, $k = 3$)

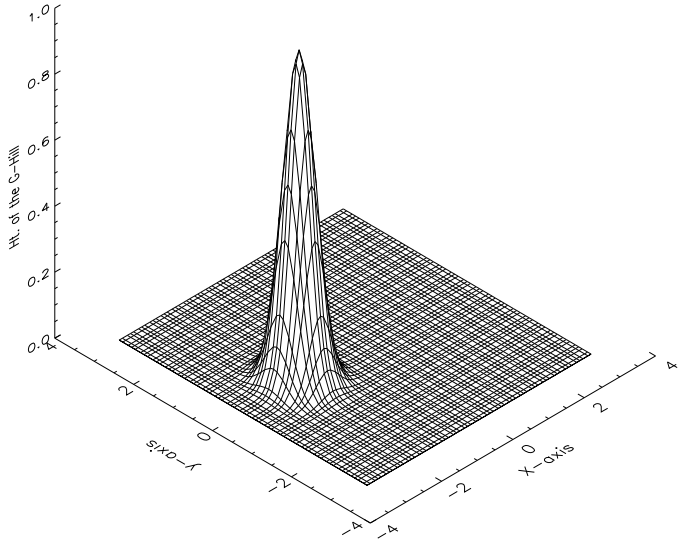

Initial solution

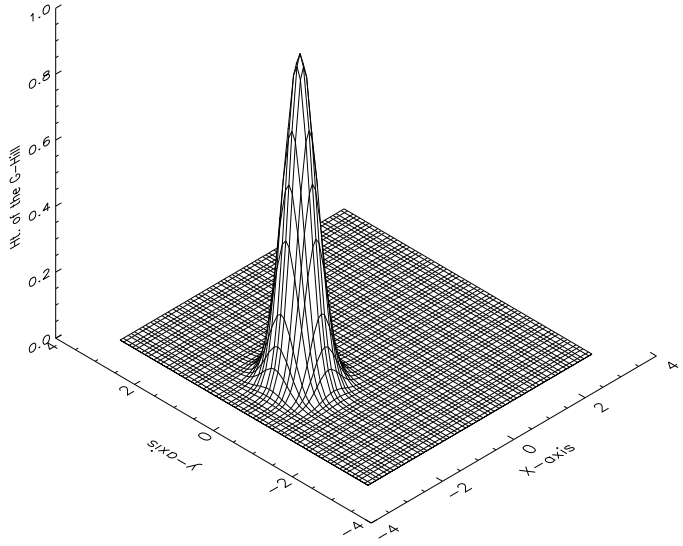

Numerical solution after one rotation

2D Cartesian: Convergence

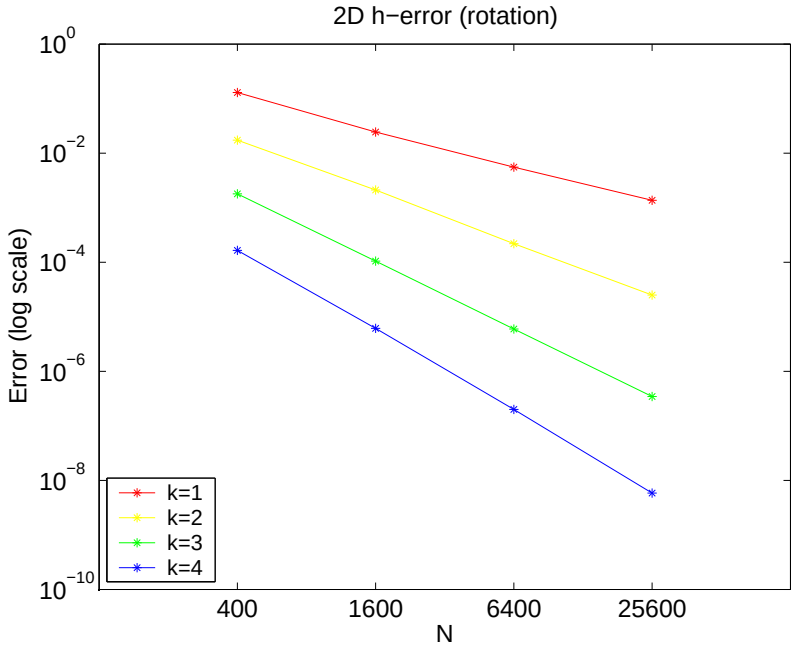

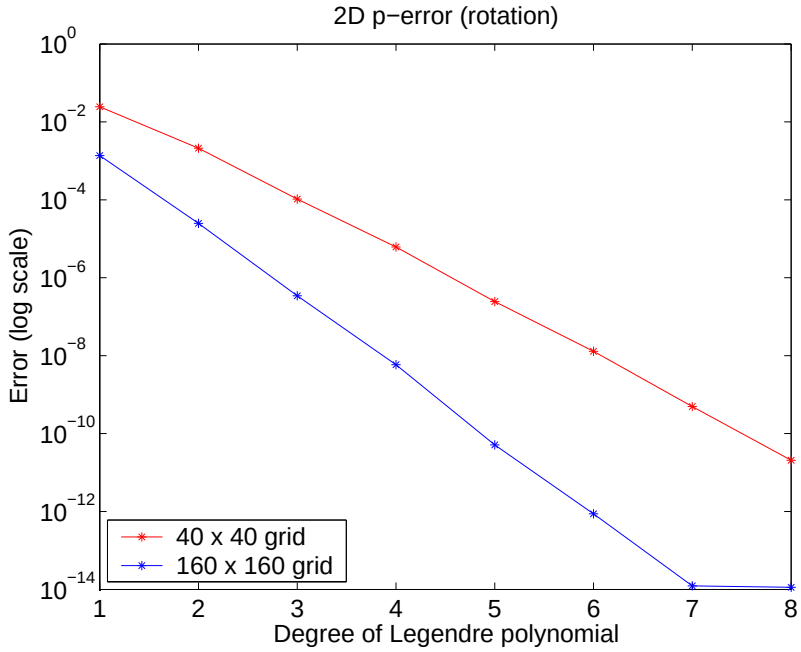

Solid-body rotation of a Gaussian-Hill

2D: Limiter Option

- Montonic option for DGM: WENO limiter

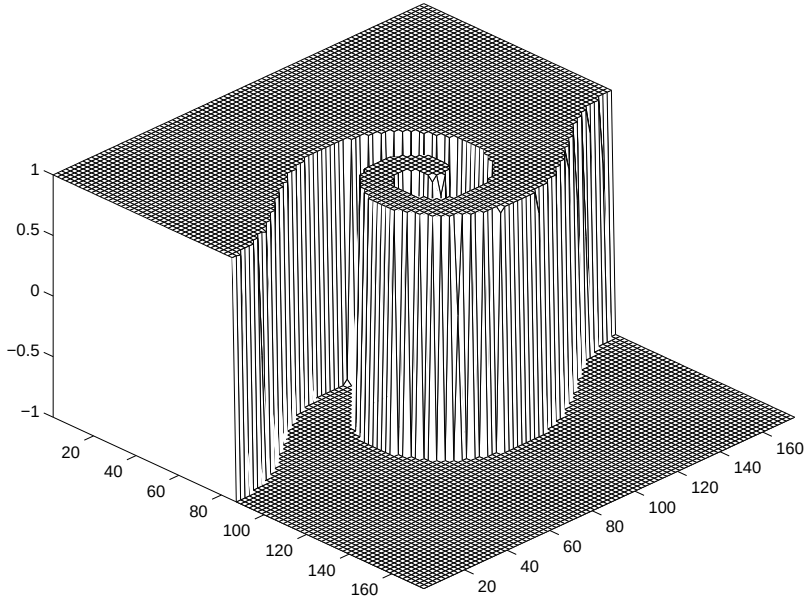

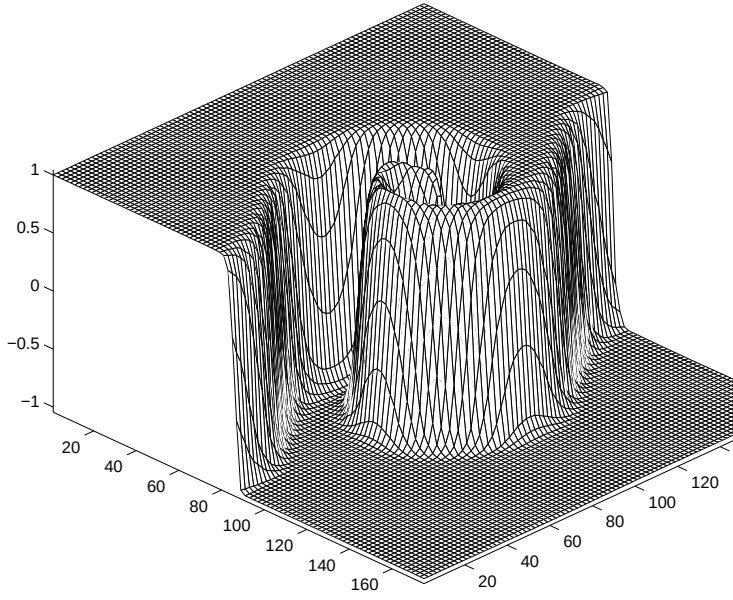

Non-smooth Vortex on a $(1600 \times 4 \times 4)$ grid. Exact vs Numerical solutions, after 3 time units

DGM: Spherical Geometry

- The sphere is decomposed into 6 identical regions, using the central (gnomonic) projection:

$$x = a \tan\lambda, \;\; y = a \tan\theta \, \sec\lambda,$$

  $2a$ is the cube side.

  - Local coordinate systems are free of singularities
  - have identical metric terms
  - creates a non-orthogonal curvilinear coordinate system

- Metric tensor of the transformation is defined as $G_{ij} \equiv \mathbf{a}_i \cdot \mathbf{a}_j$, $i, j \in \{1, 2\}$.

- The components of the covariant vectors (u_i) and the contravariant vectors (u^i) are related through:

$$u_i = G_{ij} u^j, \; u^i = G^{ij} u_j, \quad G^{ij} = (G_{ij})^{-1}$$

Equiangular Projection

Central angles $x^1, x^2 \in [-\pi/4, \pi/4]$ are the independent variables. Let $\rho^2 = 1 + \tan^2 x^1 + \tan^2 x^2$, metric tensor

$$G_{ij} = \frac{R^2}{\rho^4 \cos^2 x^1 \cos^2 x^2} \begin{bmatrix} 1 + \tan^2 x^1 & -\tan x^1 \tan x^2 \\ -\tan x^1 \tan x^2 & 1 + \tan^2 x^2 \end{bmatrix}$$

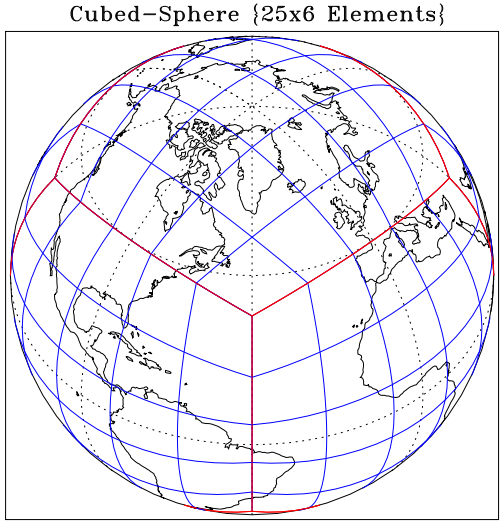

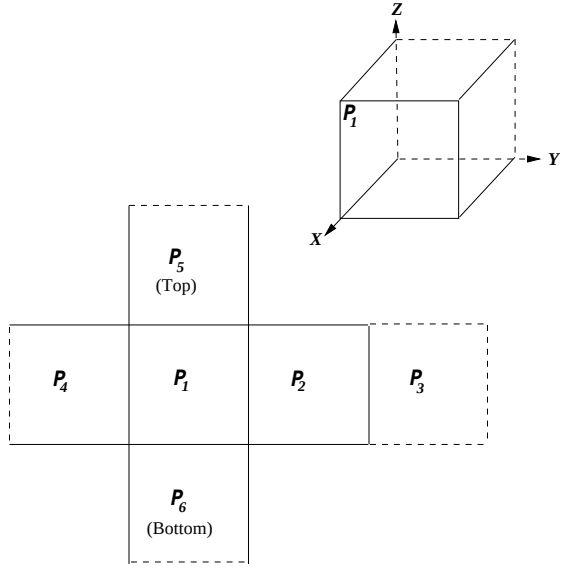

Transform: Cube $\Leftrightarrow$ Sphere

- The spherical velocity vector $\mathbf{v}(\lambda, \theta) = (u, v)$, can be expressed in terms of covariant vector $u_1 = \mathbf{v} \cdot \mathbf{a}_1$, $u_2 = \mathbf{v} \cdot \mathbf{a}_2$, $\Rightarrow \mathbf{v} = u^1 \mathbf{a}_1 + u^2 \mathbf{a}_2$.
- Metric tensor of the transformation is defined by

$$G_{ij} = A^T A; \quad A = \begin{bmatrix} R\cos\theta\, \partial\lambda/\partial x^1 & R\cos\theta\, \partial\lambda/\partial x^2 \\ R\, \partial\theta/\partial x^1 & R\, \partial\theta/\partial x^2 \end{bmatrix}$$

- The matrix A can be used for transforming spherical velocity (u, v) to the cubed-sphere velocity vectors.

$$A \begin{bmatrix} u^1 \\ u^2 \end{bmatrix} = \begin{bmatrix} u \\ v \end{bmatrix}$$

SWE on the Cubed-Sphere

In curvilinear coordinates, the continuity and momentum equations for the flux form shallow water system can be written as follows *(Sadourny 1972; Rancic et al. 1996; Nair et al. 2005 (MWR))* :

$$\begin{aligned}
\frac{\partial}{\partial t}(\sqrt{G}\,h) + \frac{\partial}{\partial x^1}(\sqrt{G}\,u^1 h) + \frac{\partial}{\partial x^2}(\sqrt{G}\,u^2 h) &= 0, \\
\frac{\partial u_1}{\partial t} + \frac{\partial}{\partial x^1} E &= \sqrt{G}\,u^2 (f+\zeta), \\
\frac{\partial u_2}{\partial t} + \frac{\partial}{\partial x^2} E &= -\sqrt{G}\,u^1 (f+\zeta),
\end{aligned}$$

where

$$G = \det(G_{ij}),\ E = \Phi + \frac{1}{2}\,(u_1\,u^1 + u_2\,u^2),\ \zeta = \frac{1}{\sqrt{G}}\left[\frac{\partial u_2}{\partial x^1} - \frac{\partial u_1}{\partial x^2}\right]$$

Flux form SWE

$$\frac{\partial}{\partial t}\mathbf{U} + \frac{\partial}{\partial x^1}\mathbf{F}_1(\mathbf{U}) + \frac{\partial}{\partial x^2}\mathbf{F}_2(\mathbf{U}) = \mathbf{S}(\mathbf{U})$$

where $\mathbf{U} = \left[\sqrt{G}\,h, u_1, u_2\right]^T$, $\mathbf{F}_1 = \left[\sqrt{G}hu^1, E, 0\right]^T$

$\mathbf{F}_2 = \left[\sqrt{G}hu^2, 0, E\right]^T$, $\mathbf{S} = \left[0, \sqrt{G}u^2(f+\zeta), -\sqrt{G}\,u^1(f+\zeta)\right]^T$.

- Each face of the cubed-sphere is partitioned into $N_e \times N_e$ rectangular non-overlapping elements Ω_{ij}
- Each element is mapped onto the reference element $[-1,1] \otimes [-1,1]$
- Total number of elements on the cubed sphere is $6 \times N_e \times N_e$.

Computational Domain

Cubed-Sphere ($N_e = 5$) with 8×8 GLL points

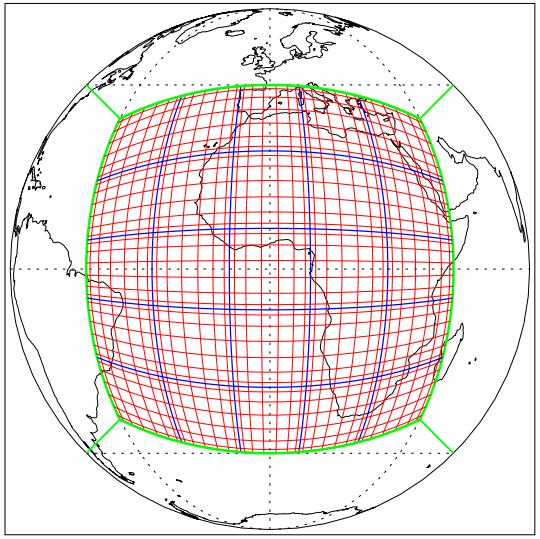

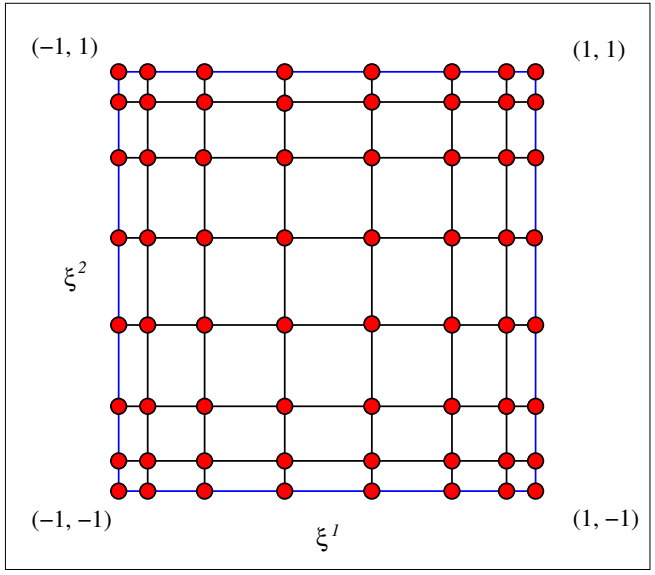

- SWE test suite by *Williamson et al. (1992, JCP)*.

Flux computation at cube edges

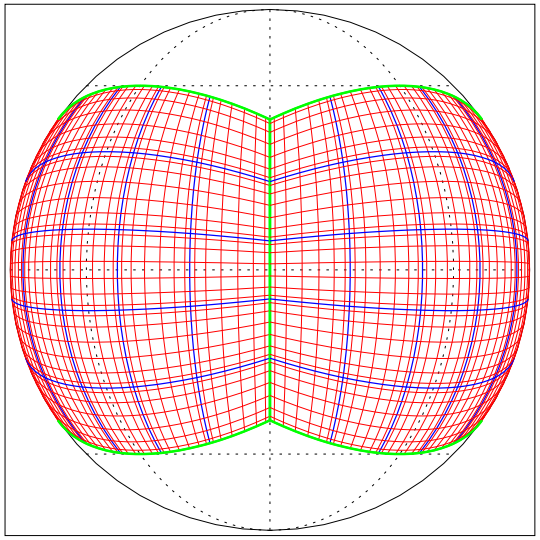

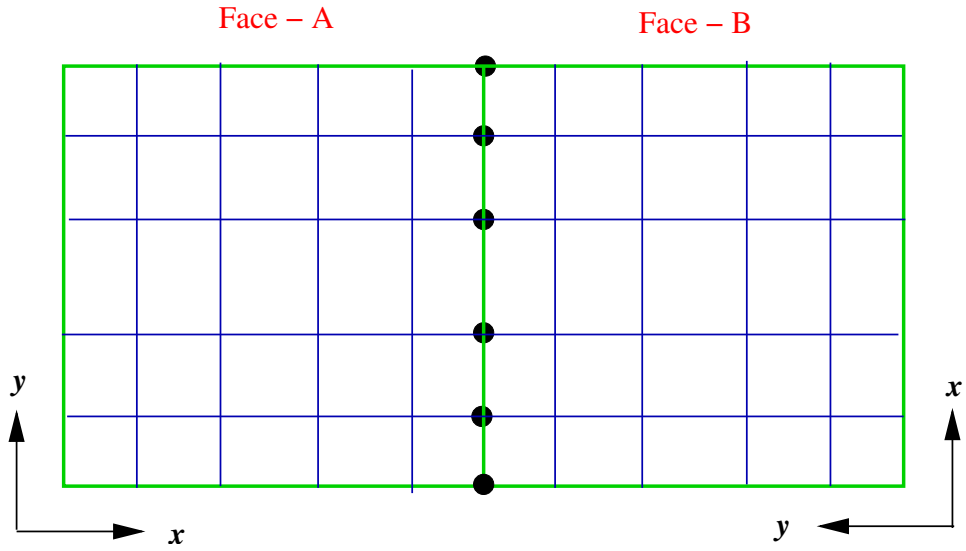

To compute the flux on the edge of the cubed-sphere, P_n, both the *left* and *right* components F_n^- and F_n^+ are required.

$$A_l \begin{bmatrix} F_l^+ \\ G_l^+ \end{bmatrix} = \begin{bmatrix} F_s^+ \\ G_s^+ \end{bmatrix}, \quad A_n^{-1} \begin{bmatrix} F_s^+ \\ G_s^+ \end{bmatrix} = \begin{bmatrix} F_n^+ \\ G_n^+ \end{bmatrix} \quad \Rightarrow \quad A_n^{-1} A_l \begin{bmatrix} F_l^+ \\ G_l^+ \end{bmatrix}.$$

SW Test-1

- Numerical Flux: Lax-Friedrichs; eigenvalues of $\mathcal{F}'(U)$

$$\alpha^1 = \max\left(|u^1| + \sqrt{\Phi\, G^{11}}\right), \quad \alpha^2 = \max\left(|u^2| + \sqrt{\Phi\, G^{22}}\right)$$

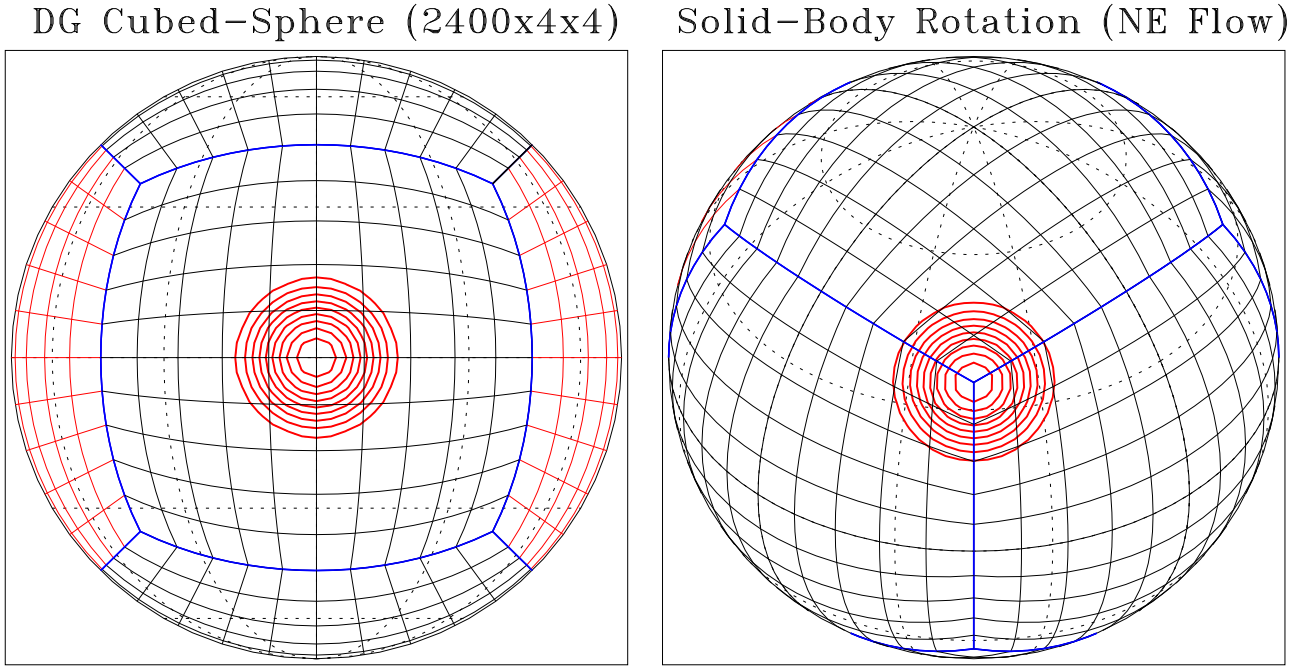

SW Test case-1: Solid-body rotation of a cosine-bell ($\alpha = \pi/4$)

SW Test-1: Modal & Nodal

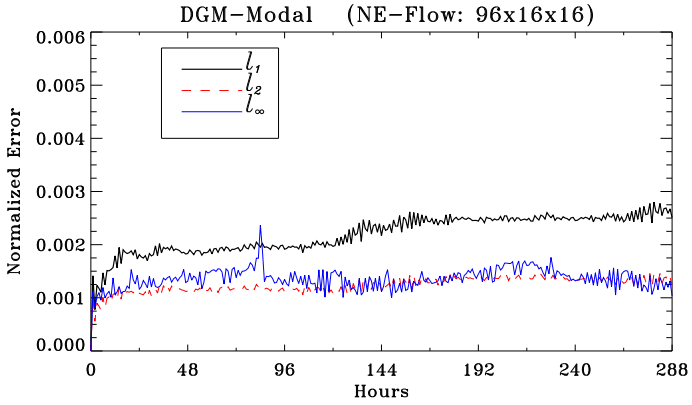

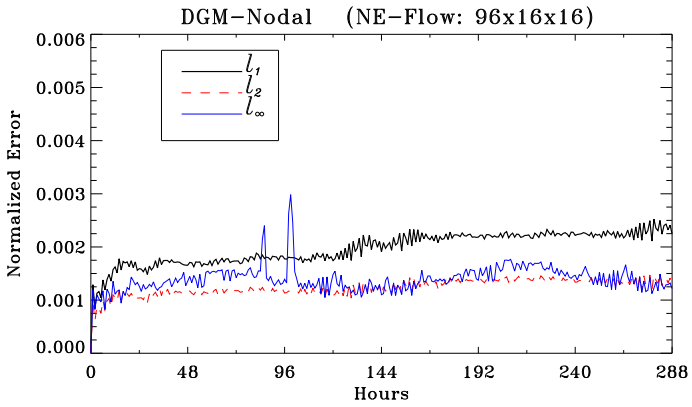

Modal vs Nodal

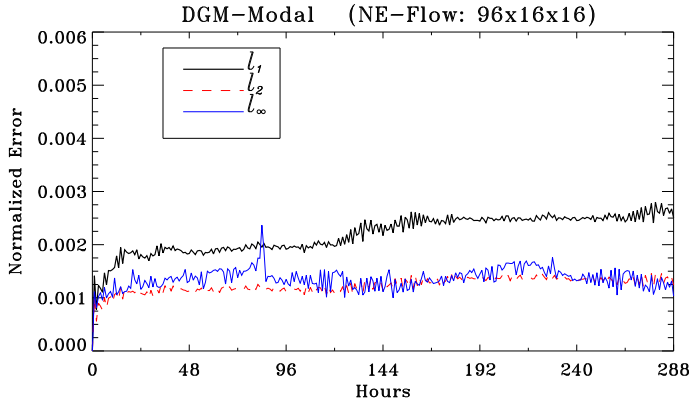

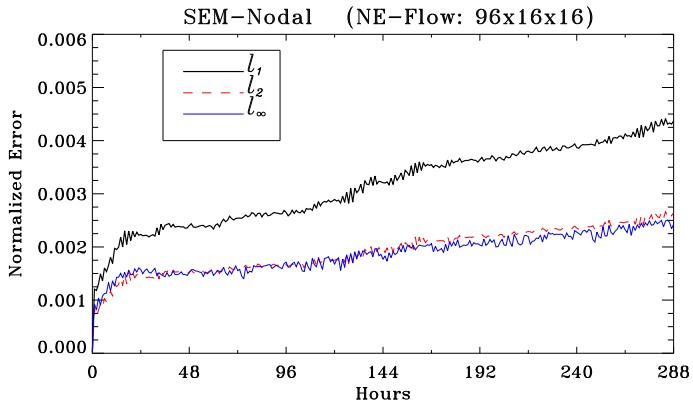

DGM vs SEM

SW Test-1: Movie

SW1 Movie

Deformational Flow

Idealized Cyclogenisis: (*Doswell 1985; Nair et al. 1999*).

$$\psi(\lambda', \theta', t) = 1 - \tanh\left[\frac{\rho'(\theta')}{\gamma}\sin(\lambda' - \omega' t)\right]$$

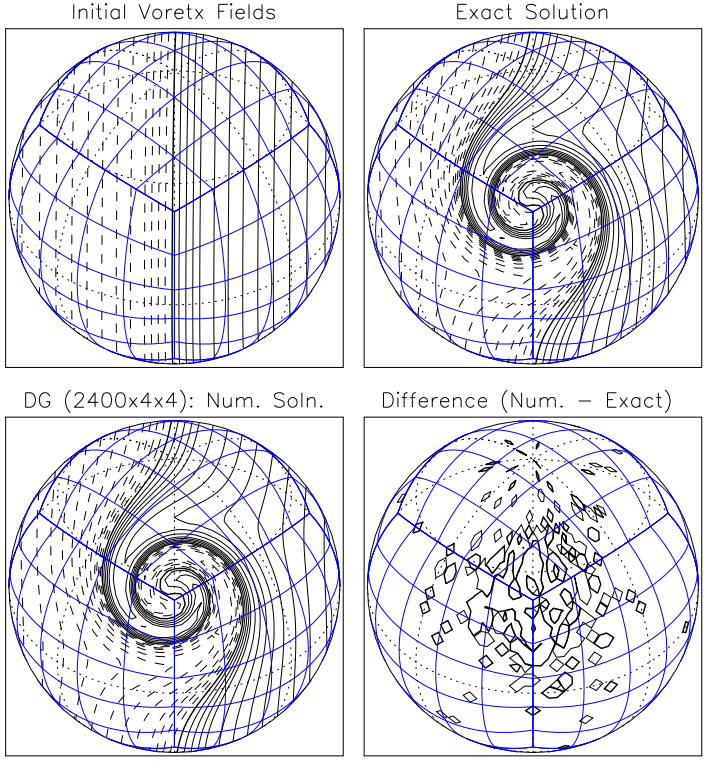

Max error is $\mathcal{O}(10^{-6})$.

Deformational Flow

Voretx Movie

SW Test-2: Geostrophic Flow

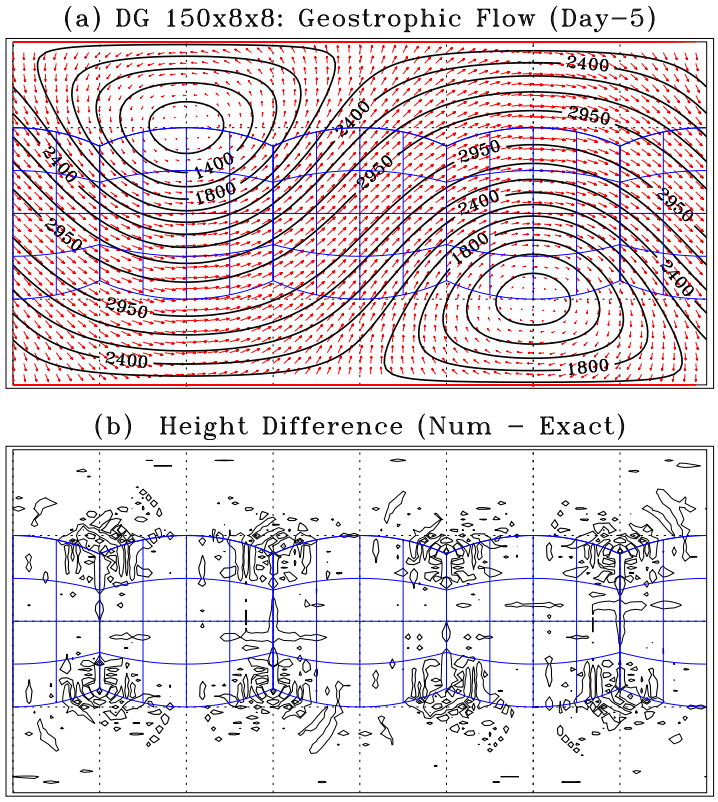

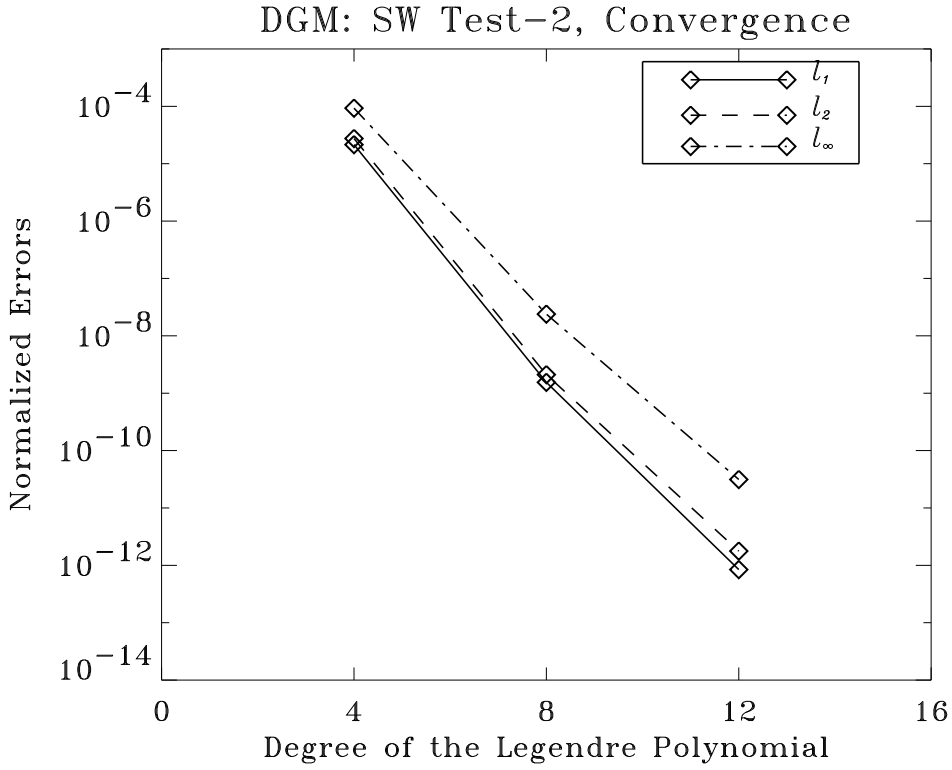

Steady state geostrophic flow ($\alpha = \pi/4$). Max height error is $\mathcal{O}(10^{-6})$ m.

SW Test-5: Flow over a mountain

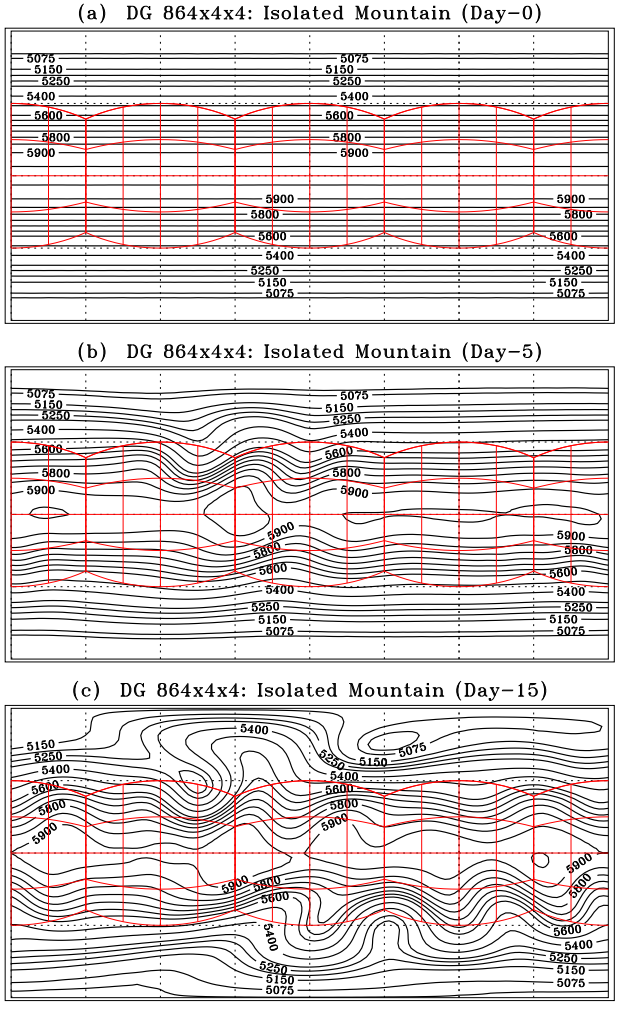

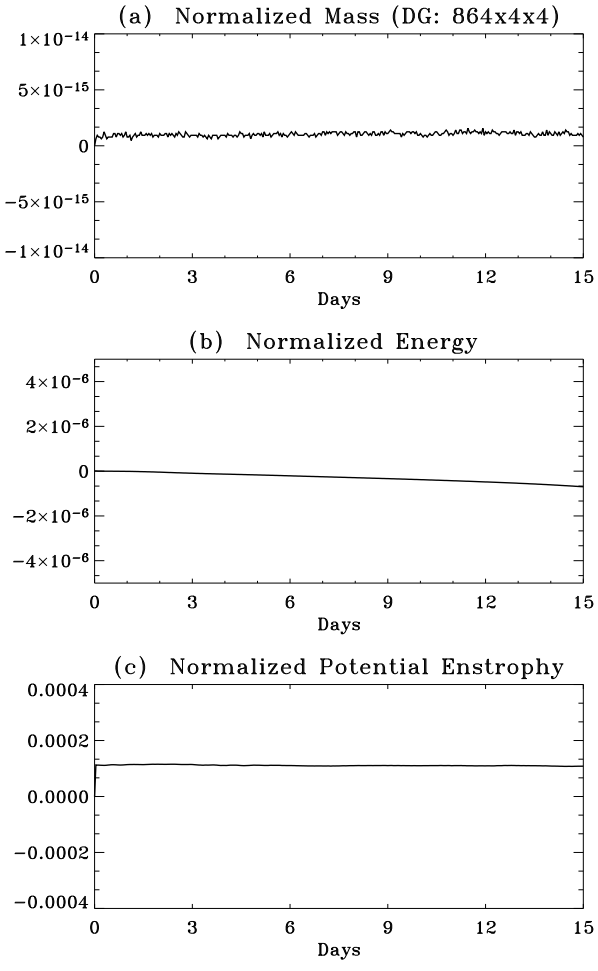

Zonal flow over a mountain: $(864 \times 4 \times 4)$ grid, after 5 and 15 days of integration

SW5 Movie

SW5 Movie

SW Test-6: Rossby-Haurwitz Wave

(a) Rossby–Haurwitz Wave (Day–0)

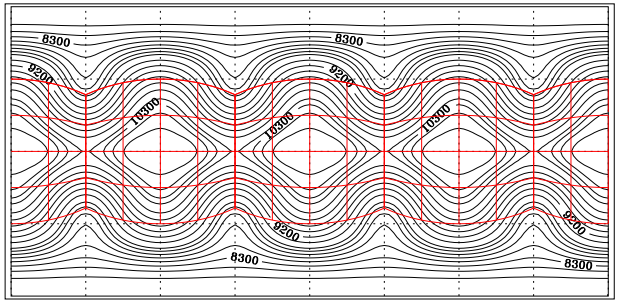

(b) Rossby–Haurwitz Wave (Day–7)

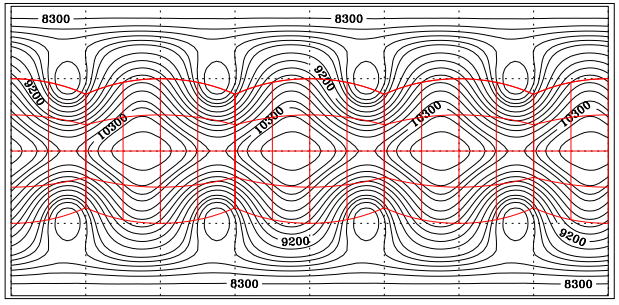

(c) Rossby–Haurwitz Wave (Day–14)

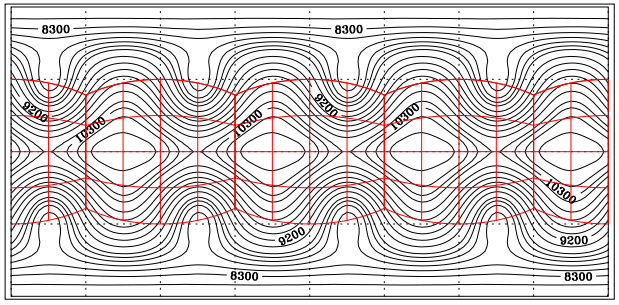

$(864 \times 4 \times 4)$ Grid.

SW6 Movie

SW6 Movie

Parallel Performance

- Strong Scaling: Hold total work constant, increase number of processes.
  - Expect to cut runtime in half by doubling process count.
  - In reality, computation time decreases but communication time remains approx. constant.
- Weak Scaling: Hold work per process constant, regardless of process count.
  - Expect runtime to remain constant, regardless of process count.
  - Since computation time remains constant, communication time has similar effect at all process counts.
- Primarily interested in strong scaling.

Performance - Hemisphere

- Linux cluster with 64 DP nodes, Intel Xenon 2.4 GHz, 8×8 Dolphin torus

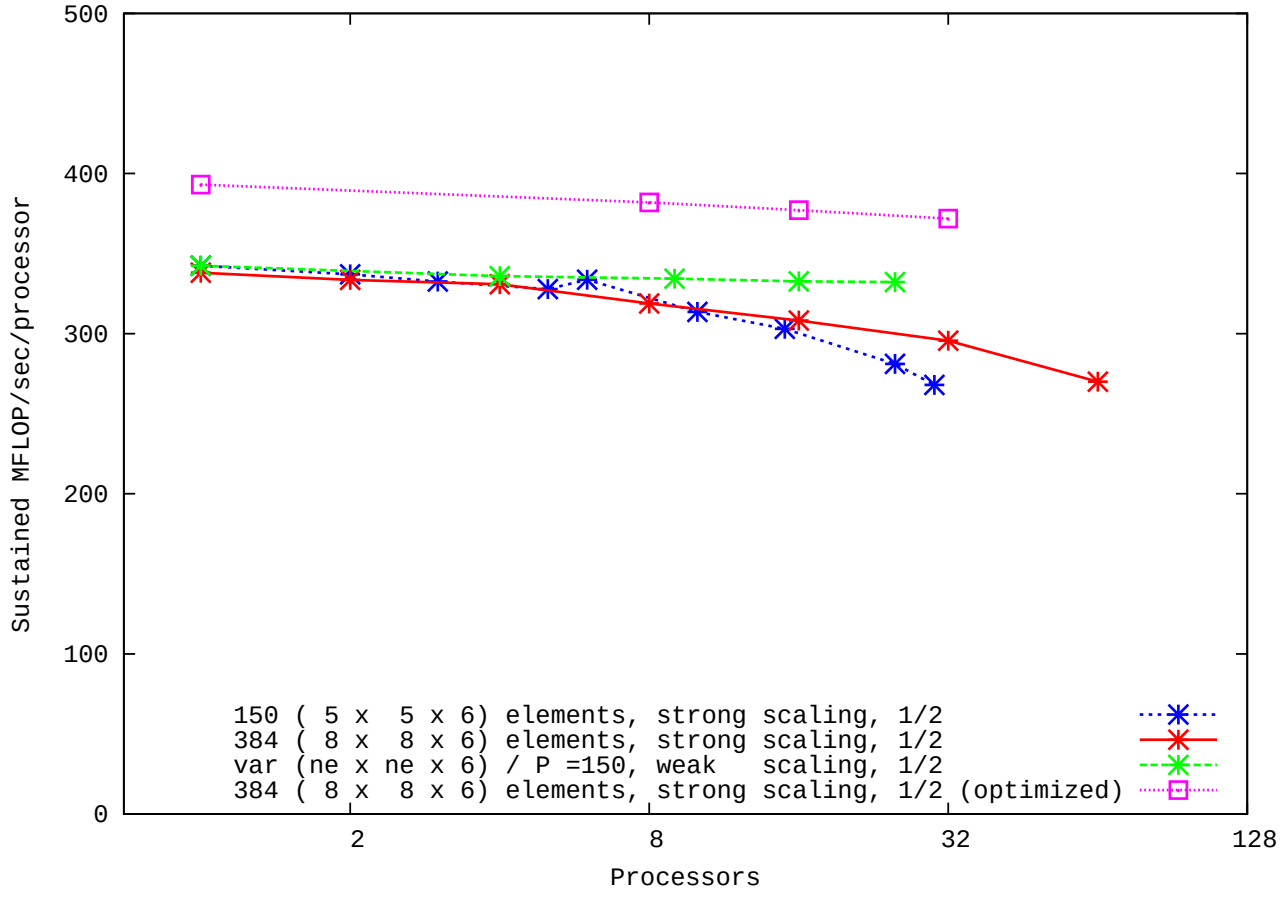

Note: 350 Mflop/Sec $\approx 14.5\%$ peak

Performance - Frost

- IBM BG/L, 1024 DP nodes, 700 MHz PPC 440s, $8 \times 8 \times 16$ torus and tree

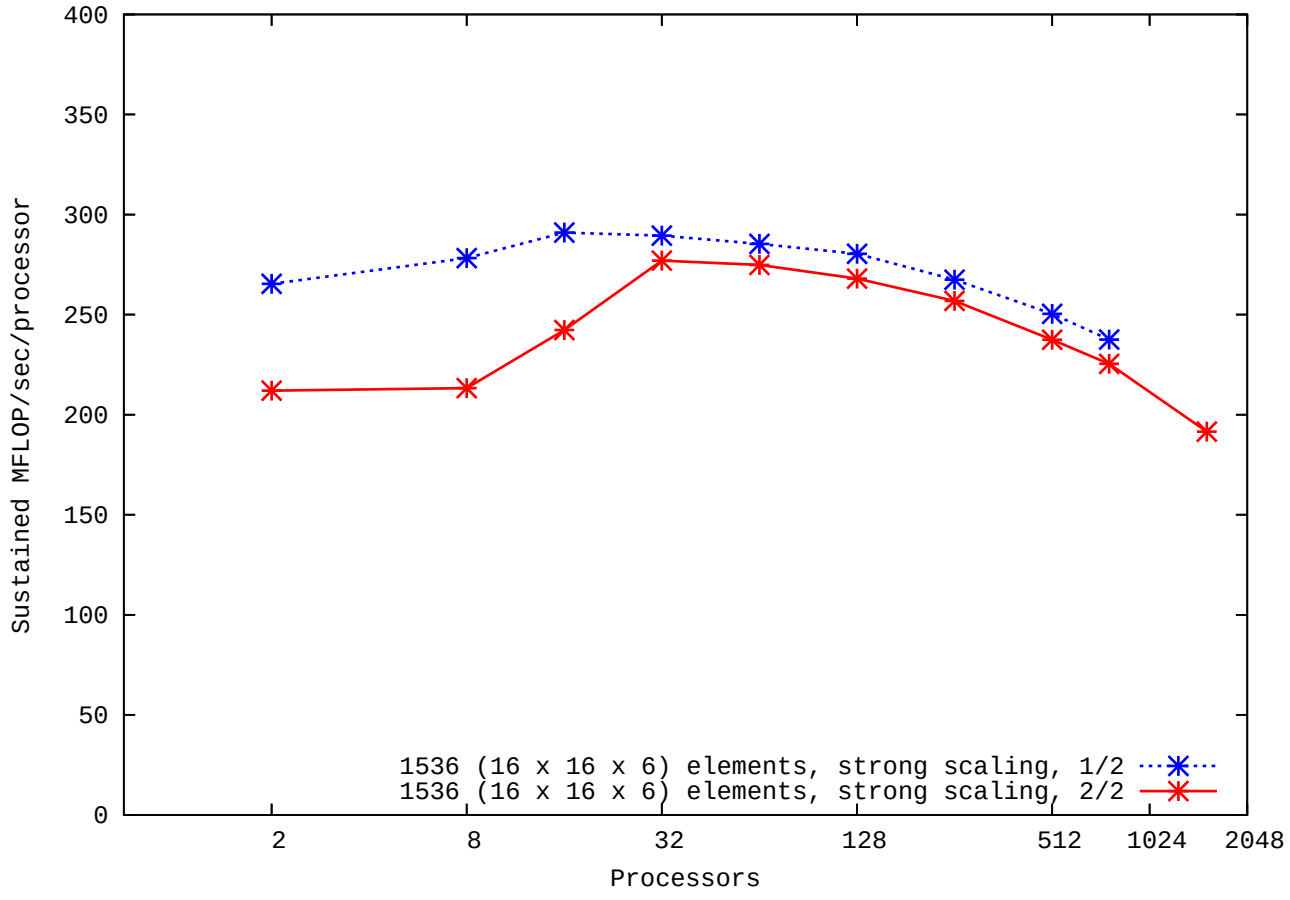

Note: 225 Mflop/Sec $\approx 8.0\%$ peak

Summary

- Discontinuous Galerkin Method (DGM) based flux form shallow water model has been developed on the cubed-sphere (*Nair et al. 2005 (MWR)*)
- Both modal and nodal versions give almost identical results
- The DG model has been implemented in NCAR high-order method modeling (HOMME) frame work.
- Numerical results either comparable or better than a standard spectral element method and DG scheme exhibits exponential convergence for SW test case-2
- DG solutions of the SW test cases are much better than those of a spectral model *(Jacob-Chien et al. 1995)* for a given spatial resolution.

Summary

- For high-order spatial discretization, the solution do not exhibit spurious oscillation for the flow over a mountain test case.
- DG model conserves mass to machine precision. Conservation of total energy and enstrophy is better preserved than the existing finite-volume models.
- Initial scaling results are promising.
- Future work: Development of a 3D DGAM dynamical core, efficient time integration scheme, limiters, performance study on BG/L.